The Circadian Clock is Essential for the Crosstalk of VEGF-Notch-mediated Endothelial Angiogenesis in Ischemic Stroke

Yuxing Zhang
Hunan University of Chinese Medicine
Xin Zhao
Hunan University of Chinese Medicine
Chun Guo
The First Affiliate Hospital of Hunan University of Chinese Medicine
Ying Zhang
Hunan University of Chinese Medicine
Fukang Zeng
Hunan University of Chinese Medicine
Qian Yin
Hunan University of Chinese Medicine
Zhong Li
The First Affiliate Hospital of Hunan University of Chinese Medicine
Le Shao
The First Affiliate Hospital of Hunan University of Chinese Medicine
Desheng Zhou (zds1101@foxmail.com)
The First Affiliate Hospital of Hunan University of Chinese Medicine
Lijuan Liu
The First Affiliate Hospital of Hunan University of Chinese Medicine

Research Article

Keywords: Circadian clock, Ischemic stroke, Angiogenesis, VEGF, Notch pathway

Posted Date: July 20th, 2022

DOI: https://doi.org/10.21203/rs.3.rs-1843132/v1

Abstract

Ischemic stroke is a major public health problem in China. Angiogenesis plays an essential role in the rehabilitation of ischemic brain injury. Recent studies demonstrated that the circadian clock is involved in the process of ischemic stroke, however, the exact mechanism of the circadian clock in regulating angiogenesis after cerebral infarction remains unclear. In the present study, we determined that environmental circadian disruption (ECD) could increase the stroke severity and impair the ability of angiogenesis in a transient middle cerebral artery occlusion (MCAO) rat model, by detecting the rat's infarct volume, neurological test, and western blot of angiogenesis-related protein, including vascular endothelial growth factor (VEGF), matrix metalloproteinase-2 (MMP-2). We further report that the core circadian clock, aryl hydrocarbon receptor nuclear translocator-like 1 (BMAL1, also known as ARNTL1), plays an irreplaceable role in angiogenesis. Overexpression of BMAL1 promotes tube forming, migration, and wound healing capacity, and upregulate the VEGF and Notch pathway protein level. While this kind of promoting effect is reversed by the Notch pathway inhibitor, DAPT, according to the results of angiogenesis capacity and VEGF pathway protein level. In conclusion, our study reveals the intervention of ECD in angiogenesis in ischemic stroke and further identifies the exact mechanism by which BMAL1 regulates angiogenesis through the VEGF-Notch1 pathway.

1 Introduction

Stroke is the second leading cause of death worldwide and the leading cause of death in China [1–3]. As the country with the heaviest burden of stroke in the world, China has more than 2 million new stroke cases annually [4]. According to the results of the 2012–2013 National Stroke Epidemiological Survey of 480,687 people (aged 20 or older) in 31 provinces, the age-standardized prevalence, morbidity, and mortality of stroke were 1114.8 per 100,000, 246.8 and 114.8 per 100,000, respectively [5]. Unfortunately, only 3–5% of acute cases can be treated with thrombolytic tissue plasminogen activator (tPA), which is the only treatment approved by the Food and Drug Administration(FDA) [6].

Previous studies reported that repair of the damaged neurovascular unit (NVU), especially angiogenesis, contributes to the establishment of collateral circulation and plays a pivotal role in the recovery of ischemic stroke injury [7, 8]. Angiogenesis is a complex process in which a large number of substances are released to participate in angiogenesis after ischemic stroke. Hypoxia-induced angiogenesis, which occurs in the ischemic penumbra within hours of stroke and persists for several weeks [9], is one of the major events in adaptation to glucose deficiency and hypoxia and is critical for maintaining cell metabolism, survival, and function [10, 11].

After stroke, ischemic penumbra tissue releases angiogenesis factors, including vascular endothelial growth factor (VEGF), matrix metallopeptidases (MMPs), platelet-derived growth factor (PDGF), angiogenin (Ang), which promote the basement membrane (BM) degeneration, extracellular matrix (ECM) remodeling, endothelial cells (ECs) proliferation and migration, resulting in the formation of neovascularization, thereby improving collateral circulation [12, 13]. Clinical studies have confirmed that

patients with high cerebrovascular density have better functional recovery and longer survival time than those with low cerebrovascular density [14–16]. Therefore, promoting angiogenesis in patients has gradually become a promising strategy for the treatment of ischemic stroke.

Circadian rhythms are endogenous oscillations at the cellular level, with a period of approximately 24 hours, that regulate the metabolic and behavioral output of cells [17]. Circadian rhythms determine cell fate, including neurons, glia, endothelial, neutrophils, macrophages, which are involved in the angiogenesis, the immune response process in ischemic stroke [18, 19]. Recent studies have shown that circadian rhythm significantly affects the susceptibility, injury, recovery, and treatment response mechanism of stroke [20]. Shift work-induced environmental circadian disruption (ECD) increases stroke severity and immune response dysregulation [21]. As for angiogenesis, studies found that the circadian rhythm transcription factor Bmal1 (aryl hydrocarbon receptor nuclear translocator-like 1) was confirmed to have a positive regulatory effect on the increase of VEGF-A, a key molecule induced by hypoxia-induced angiogenesis, but a negative regulatory effect was observed in Period2 (Per2), cryptochrome1 (Cry1) [22, 23], and further researches proved that BMAL1 directly binds to the promoter region of the VEGF and regulates the promoter activity [24].

Several studies have shown that the Notch signaling pathway may interact with VEGF under hypoxic conditions to jointly regulate arterial properties and angiogenesis [25]. Preliminary research on VEGF and Notch pathways comes from the study of vasculogenesis. The results suggest that VEGF plays a role in arteriogenesis and angiogenesis by regulating the expression of Notch1 and Dll4 in the upstream of Notch pathway [26, 27]. Furthermore, in stroke models, the Notch signaling pathway is involved in the formation of collateral networks in ischemic stroke. Inhibition of Notch signaling can affect tissue perfusion by restricting arterial structure and function, impairing the repair of angiogenesis after ischemia. [28, 29].

The present study aimed to investigate the effect of circadian rhythms on hypoxia-induced collateral vessel formation after ischemic stroke and the potential proangiogenic mechanism of the core circadian genes. Therefore, we constructed a rat middle cerebral artery occlusion (MCAO) and environmental circadian disruption (ECD) model, and a mouse brain microvascular endothelial cells (bEnd.3) oxygen-glucose deprivation/reoxygenation (OGD/R) model in this research. We further determined the relationship between ECD and angiogenesis after ischemic stroke, and the role of Bmal1 on the angiogenic process after OGD/R intervention. These results suggested that ECD can significantly increase the severity of ischemic stroke, impair the ability of angiogenesis, and reduce neurological recovery. The core clock gene Bmal1 has also been confirmed as a potential therapeutic target to promote angiogenesis after ischemia-hypoxic injury by regulating the expression of VEGF and Notch signaling pathways.

2 Methods And Materials

2.1 Ethics statement

All animal experiments were performed in accordance with the guidelines of the China Council on Animal Care and Use. This study was approved by the Laboratory Animal Professional Committee of the First Affiliated Hospital of Hunan University of Chinese Medicine (Approval no. 20201010-13). Every effort was made to minimize pain and discomfort to the animals. Animal experiments were performed in The First Affiliated Hospital of Hunan University of Chinese Medicine. All rats were kept in cages with suitable temperature (23–25℃) and humidity (40–60%), and were randomly divided into 3 groups. Rats have unrestricted access to food and water.

2.2 Circadian Disruption Protocol

Sprague Dawley rats were used in this experiment. Before intervention, rats were housed for 2 weeks to acclimate to housing facilities and handling. The rats were then randomly assigned to various experimental groups, and they were kept in cages for the rest of the study. Rats were assigned to a standard 12:12 LD schedule (n = 40) or a chronic LD shift schedule (n = 20) for a 44-day (6 weeks) of light intervention (Fig. 1A). This lighting schedule causes environmental circadian disruption (ECD), which has been cited in many articles [21, 30, 31]. In this timetable, by advancing the dark cycle, the 12:12 LD cycle was advanced by 6 hours, once every 7 days. Rats were given standard rat food after arriving at the facility. Rat food and water are freely available to animals.

2.3 Middle cerebral artery occlusion and reperfusion (MCAO/ R) model

The MCAO procedure was scheduled on the last day of week 6 of the ECD protocol. Considering the difference of illumination time, MCAO operation of ECD group was performed at 6:00–12:00, and Ctrl group was performed at 12:00–18:00. The rats fasted for 12 hours before the operation, but they were still free to drink water during this period. The anesthetized rats were placed in a supine position on a scaffold, under sterile conditions, the right common carotid artery (CCA), external carotid artery (ECA), internal carotid artery (ICA), and the junction of the carotid artery were carefully exposed through a midline neck incision. A silicon-coated suture (head diameter 0.36 ± 0.02 mm, Beijing Senbi Biotechnology Co., Ltd., Beijing, China) was inserted into the external cervical incision, and the blood flow was blocked for 2 hours through the ICA to the beginning of the middle cerebral artery, reperfusion was simulated by removing the suture. Maintain the temperature at 37 ± 0.5°C with a thermostatic surgical pad. After the operation, all rats were placed on a warm blanket until recovery.

2.4 Neurological Tests

Neurological deficits were evaluated by a blinded observer using an 18-point scoring system 24 h after reperfusion, and completed within the first 2 hours after illumination was initiated with subsequent 3d, 7d, and 10d, respectively. Scores of 18 were according to the following six tests: spontaneous activity, limb symmetry, forepaw outstretching, climbing, body proprioception, and response to vibrissae touch. Each score was the total of scores for each of the six tests (minimum score, 3; maximum score, 18).

2.5 Triphenyl-tetrazolium chloride (TTC) staining

The TTC was performed 24h after operation in each group. Brain tissues in each group were frozen at -20°C for 20 min. Then the brain was sliced into 2-mm-thick coronal slices and immediately stained with phosphate-buffered saline (PBS; Procell, Wuhan, China) containing 2% TTC (Sigma, Saint Louis, MO, USA) in a 37℃ incubator for 30 minutes, fixed with 4% paraformaldehyde and photographed. The infarct areas appeared white while the normal ones were red. The cerebral infarction ratio was measured by Image-Pro Plus software (ie. the percentage of the area of the infarct area to that of the homolateral cerebral hemisphere).

2.6 Cerebral histopathology (HE staining)

After 24 h of reperfusion in each group, rat brain samples were collected into cryovials containing 4% paraformaldehyde. The samples were dehydrated and embedded in paraffin, and coronal sections were prepared. These sections were then stained with hematoxylin and eosin (HE) and used for study histopathology. Finally, images were acquired by light microscopy (Leica, Wetzlar, Germany) to assess histopathological changes in hippocampal tissue.

2.7 CD34 immunofluorescence staining of rat hippocampus and cortex

The presence of CD34 in the hippocampus and cortex of each group was detected by immunofluorescence 10 days after reperfusion. To minimize the factor of the endogenous circadian phase, the timing of brain sampling in Ctrl and MCAO groups were conducted during 6:00–12:00, while the MCAO-ECD group was 12:00–18:00. Coronal sections were collected and prepared as described in 2.6. Before staining, sections were deparaffinized and rehydrated, and antigen retrieval was performed. Afterwards, sections were blocked with 5% BSA for 1 h at room temperature. Then, the slices were incubated at 4℃ overnight with anti-CD34 (ab81289, Abcam,1:200). Next day, the slices were washed 3 times with PBS and incubated with CoraLite594 (SA00013-4, Proteintech, 1:400) for 2 h at room temperature. After rinsed, the nuclei were stained with DAPI for 15min. The number of immunoreactive cells in predefined areas was quantified using ImageJ software (NIH, Bethesda, MD, USA). Cells were counted in three different fields of view for each mouse in each group of three mice. All counts were performed by blinded observers.

2.8 ELISA of Melatonin, VEGF, IL-1β, IL-18 and TNF-α

The timing of serum sampling in each group is the same as described in 2.7. Blood samples were taken from the abdominal aorta in Ethylenediaminetetraacetic acid (EDTA)-containing tubes and the plasma was separated. The concentrations of melatonin, VEGF, IL-1β, IL-18, and TNF-α in plasma samples in both groups were measured by ELISA Complete Kit (Cusabio Biotech, Wuhan, China) according to the manufacturer's protocol using an Elisa reader to record OD. The final concentrations of melatonin were calculated based on a standard curve constructed using hormone standards. Each sample was evaluated in triplicate and the mean concentration was used for further analysis.

2.9 Cell circadian gene induction and OGD/R treatment

bEnd.3 cells (mouse brain microvascular endothelial cells) were donated by Dr. Yan Shang, for which we are very grateful. bEnd.3 cells were cultured in Dulbecco's Modified Eagle Medium (DMEM; Procell, Wuhan, China) supplemented with 10% fetal bovine serum (FBS; Procell, Wuhan, China), 1% penicillin, and streptomycin, and placed in an incubator with 5% CO_2 at 37°C. bEnd.3 cells were sub-cultured when the cell density reached 90%. Finally, the cells used for the subsequent experiments were in the logarithmic growth phase.

To synchronize the circadian gene rhythmically expression, bEnd.3 cells were cultured in complete medium containing dexamethasone (100nM) for 2h [32, 33]. Then cells were harvested or subjected to OGD at the indicated time points. Before OGD treatment, the culture medium was replaced with glucose-free DMEM and incubated for 6h at 37°C in an atmosphere of 5% CO2 and 95% N2. Afterward, replace the glucose-free medium with complete medium, put the cells back into the incubator (with O_2) for 24 hours.

2.10 DAPT treatment

To verify the proportion of the Notch1 signaling pathway in vitro study, DAPT (HY-13027, MCE, Princeton, NJ), a kind of gamma-secretase inhibitor, was used in this study. DAPT inhibits the formation of soluble Notch intracellular domain (NICD) proteins by preventing γ-secretase cleavage at the S3 site of the Notch receptor, preventing NICD translocation to the nucleus. Before OGD intervention, bEnd.3 cells were incubated in serum-free medium in the presence or absence of 10 μM DAPT for 24h. The DAPT intervention group continued to intervene during the OGD process and after the end of OGD until the end of each experiment, including scratch wound assay, migration assay, and tube formation assay.

2.11 Bmal1 overexpression and knockdown lentivirus vector infection

The overexpression of lentivirus vector was Constructed by Genechem (Genechem Co., Ltd., Shanghai, China). The sequence used for PCR amplification of Bmal1 is shown below: Arntl-21735-P1:AGGTCGACTCTAGAGGATCCCGCCACCATGGCGGACCAGAGAATGGACATTTC; Arntl-21735-1-P2:TCCTTGTAGTCCATACCCAGCGGCCATGGCAAGTCACTAAAG. And the Bmal1 siRNA Lentivirus vector construction and packaging services are provided by Hanbio (Hanbio Co., Ltd., Shanghai, China). Interference target design and primers are shown as follows: siRNA1: GCTTGTTTGACTACCTGCATCCAAA; siRNA2: CGGGTGAAATCTATGGAGTACGTTT; siRNA3: CAGTAACGATGAGGCAGCAATGGCT.

bEnd.3 cells were prepared as suspension and inoculated into a 6-well plate with $5–8×10^4$ per well for 24-36h. Once they reached the 35–50% density, a suitable volume of the lentivirus infection reagent was added to culture medium according to MOI = 30. After 24hours, the medium was replaced with a complete medium. At 72 hours after transfection, the transfection efficiency was determined by the expression of green fluorescent protein (GFP). Then, the bEnd.3 cells were sub-cultured in medium containing 6 μg/ml puromycin for 7 days until the transfection efficiency reached more than 95%. The single transduced stable cell line was established and used for all subsequent cell cultures and each experiment after transduction.

2.12 Chromatin immunoprecipitation sequencing (ChIP-seq)

Approximately 3×10^7 bEnd.3 cells were cross-link with 1% formaldehyde for 20 min when the confluency reached 90%. The crosslinking reaction was quenched by adding glycine to a final concentration of 125 μM. After washing with cold PBS for three times, nucleus lysate exaction was collected by centrifugation and resuspended in 300 uL of nuclear lysis buffer (50 mM Tris-HCl pH 8.0, 1% SDS, 10 mM EDTA). After centrifugation at 17,000 rpm for 15 minutes at 4°C, the fragmented chromatin was diluted 1:5 with IP dilution buffer (20 mM Tris-HCl pH 8.0, 150 mM NaCl, 1% Triton X-100, 1 mM EDTA) supplemented with 1x protease inhibitor cocktail, and incubated with 10 μg anti-Bmal1 (ab230822, Abcam) overnight at 4°C. 100 μl of Dyna bead Protein A (Invitrogen 10002D) was added and incubated for another 3 h. After washing for 3 times,200μl of direct elution buffe was applied to the bead pellet along with RNAse A and reverse crosslinked at 65°C overnight. Then proteinase K was applied and incubated at 55°C for 2 h. Finally, DNA was purified by the following deep sequencing (ChIP-seq) (SeqHealth Tech, China). For ChIP-seq results, after obtaining raw sequencing data (raw data), it is filtered and high-quality sequencing data (clean data) is subjected to further comparative analysis. The results were then compared with genome-wide de novo peak calling to investigate the binding preferences of proteins across the genome, and motif analysis of binding sites was performed.

2.13 Dual-luciferase reporter assay

To study the potential regulation mechanism by which Bmal1 performs its biological function in endothelial cells, dual-luciferase reporter assay was performed. Wild-type Notch1 promotor (PGL3-Basic-H-Notch1-WT) plasmid and Mutant-type Notch1 Promo-tor (PGL3-Basic-H-Notch1-MT) were constructed by PGL3-Basic-Vector, overexpression of Bmal1 plasmid (GTP-H-Bmal1) was constructed by GTP Vector. Then, 293T cells were co-transfected with PGL3-Basic-H-Notch1-WT, PGL3-Basic-H-Notch1-MT, and NC vector or GTP-H-Bmal1 and cultured for 48 h. Finally, the Luciferase activity of cells was measured, with the fluorescence value of Renilla plasmids as the internal reference (Promega, Madison, WI, USA).

2.14 Cell viability assay by cell counting kit-8 (CCK-8)

Cell proliferation was detected by the CCK-8 assay according to the manufacturer's protocol (Cell Counting Kit-8, Apply Gen, China). bEnd.3 cells were inoculated onto 96-well plates at 10^4/100μl per well and incubated at 37°C. Each group had 5 replicates and grew for 24, 48, 72, and 96 hours. 10μl of CCK-8 solution was added to each well, and the mixture received continuous incubation at 37°C for 2h. Finally, the OD450 was measured by a microplate reader (Bio-Tek Instruments, USA). The proliferation curve was drawn with the time and the corresponding OD450 values.

2.15 Immunofluorescence assays of Bmal1, VEGF, and Notch1 in bEnd.3 cells

bEnd.3 cells were seeded on slides in 24-well plates and modeled with 6h-OGD intervention. The sample was fixed with 4% paraformaldehyde for 25 minutes 24 hours after OGD treatment, then washed with TBST for three times. It was subjected to blocking with Immunol staining blocking buffer. The anti-Bmal1

(ab3350, Abcam, 1:500), anti-VEGF (ab52917, Abcam, 1:500), and anti-Notch1 (10062-2-AP, Proteintech, 1:400) antibody was incubated separately overnight at 4°C, followed by Dylight 549 goat anti-rabbit IgG H + L (A23320, Abbkine, 1:500) and Donkey Anti-Rabbit IgG H&L (ab150075, Abcam, 1:500) for 1 hour in dark environment at room temperature. Finally, the slides were incubated with DAPI solution and an anti-fluorescence quencher. The slides were detected using a fluorescence microscope (BX51TRF, Olympus, Japan). Three fields were randomly chosen in every sample, and the fluorescence intensity was analyzed using ImageJ software (NIH, Bethesda, MD, USA).

2.16 Scratch wound assay

bEnd.3 cells were plated into a 6-well plate (2×10^5 cells/well), and incubated to reach confluence. When the bEnd.3 cells density reached about 85%, they were incubated in serum-free medium for cycle synchronization, then the monolayer was scratched using the pipette tip and washed with PBS to remove the detached cells. Then the OGD treatment cells were cultured in glucose-free DMEM in an atmosphere of 5% CO2 and 95% N_2 at 37°C for 6h. After OGD treatment, all groups were cultured in complete medium for 24h, the wound healing area was observed under a microscope at 0 h and 24 h. The group using the DAPT intervention was used at the beginning of cycle synchronization and continued until the end of the experiment. The cell migration area was measured with ImageJ software, and the area was normalized to that of control cells. The closure area of the wound was calculated as follows: migration area (%) = (A0h – A24h)/A0h × 100%, where “A0h” represents the area of the initial wound area, "A24h" represents the remaining area of the wound 24 hours after the measurement point. Data were analyzed using ImageJ software (NIH, Bethesda, MD, USA).

2.17 Tube formation assay

The cycle synchronization process is described in 2.16, 50μL Matrigel matrix (BD Biosciences, San Diego, CA), was plated in 96-well plates and incubated at 37°C with gel for 30 min. A total of 2×10^4 bEnd.3 cells were suspended in glucose-free medium or complete medium and seeded on polymerized Matrigel in 96-well plates. After incubation at 37°C under OGD treatment for 6 h, tube formation was photographed, and the analysis was performed with Image J. Each experiment was repeated in three replicates. Since the initial experimental modeling time was 6 h, and the optimal tube formation timing was 6 h to 9 h, 6 h was selected as the observation time point. Therefore, DAPT in the DAPT intervention group was used at the beginning of cycle synchronization and during the OGD process. Total branch length was quantified in this experiment. The total branch length is the sum of the length of branches and segments in a graph. Data were analyzed using ImageJ software (NIH, Bethesda, MD, USA).

2.18 Migration assay

Transwell migration assay was used to evaluate the migration ability of bEnd.3 cells. The cycle synchronization process is described in 2.16. A total 2×10^4 bEnd.3 cells were seeded into the upper chamber (3422, Corning Incorporated, USA), and the bottom of the upper chamber was synthesized by a polycarbon membrane covered with pore diameters of 8μm. Both the upper and lower chambers were

filled with glucose-free DMEM. After maintaining OGD treatment for 6 hours, the medium in the lower chamber was replaced with complete medium as a chemoattractant. After incubating with 5% CO2 and 95% O2 at 37°C for 24h, the cells remaining on the upper surface of the membrane were removed. The bEnd.3 cells on the lower surface of the membrane were fixed with 4% formaldehyde and stained with 0.1% crystal violet. The DAPT-intervened group received DAPT in both upper and lower chambers during cycle synchronization, during the OGD process, and 24 hours after OGD. The stained cells were photographed and quantified by counting in five random microscopic fields and quantified by Image J software (NIH, Bethesda, MD, USA).

2.19 Real-time quantitative polymerase chain reaction (RT-qPCR)

Total RNA was isolated from each group with Ultra-Pure Total RNA Extraction Kit (SimGen, Hangzhou, China). Reverse transcription was carried out with a reverse transcription kit (Novoprotein, Shanghai, China). RT-qPCR was performed with the CFX96Touch (Bio-Rad, CA, USA) according to the manufacturer's protocol. The mRNA level of each target gene was normalized to β-actin. The primers used are shown in Table 1.

Table 1
Primer sequences for RT-qPCR.

Gene	Sequence	Accession number
BMAL1	F: 5′- AACCTTCCCGCAGCTAACAG – 3′	NM_001374642.1
	R:5′- AGTCCTCTTTGGGCCACCTT – 3′	
VEGF	F: 5′- CCAGCAGAAAGAGGAAAGAGGTAG – 3′	NM_001110267.1
	R: 5′- CCCCAAAAGCAGGTCACTCAC – 3′	
VEGFR2	F: 5′- CTACAGACCCGGCCAAACAA – 3′	NM_001363216.1
	R: 5′- CAGCTTGGATGACCAGCGTA – 3′	
ANG	F: 5′- GCAGAAGCAACAACTGGAGC – 3′	NM_001286062.1
	R: 5′- TCCTCCCTTTAGCAAAACTTCT – 3′	
MMP2	F: 5′- CCAGAAGGCGAACAGACTG – 3′	NM_001320216.1
	R: 5′- TGGGCCGGAGACCTAAAGAG – 3′	
MMP9	F: 5′- GCGTCGTGATCCCCACTTAC – 3′	NM_013599.5
	R: 5′- CAGGCCGAATAGGAGCGTC – 3′	
Notch1	F: 5′- TCAGTGGCCCTAATTGCCAG – 3′	NM_008714.3
	R: 5′- ACCTCGCAGGTTTGACCTTG – 3′	
Jag1	F: 5′- TCCTGTCCATGCAGAACGTG – 3′	NM_013822.5
	R: 5′- CAAAGTGTAGGACCTCGGCCA – 3′	
DLL4	F: 5′- TGGGACTCAGCAAGTGTGC – 3′	NM_019454.3
	R: 5′- GTAGCTATTCTCCTGGTCCTTACA – 3′	
HES1	F: 5′- CTACCCCAGCCAGTGTCAAC – 3′	NM_008235.2
	R: 5′- ATGCCGGGAGCTATCTTTCT – 3′	
HEY1	F: 5′- CTGAGCGTGAGTGGGATCAG – 3′	NM_010423.2
	R: 5′- CGCCGAACTCAAGTTTCCAT – 3′	
β-actin	F: 5'- GTACCACCATGTACCCAGGC – 3'	NM_007393.5
	R: 5'- AACGCAGCTCAGTAACAGTCC – 3'	

Note: RT-qPCR, reverse transcription quantitative polymerase chain reaction; F, forward; R, reverse.

2.20 Western blotting

Tissue and cell proteins were extracted according to the instructions of the Enhanced Ripa cracking liquid (ApplyGEN, Beijing, China), then the protein concentration was measured and balanced among the different samples. After adding the 5× loading buffer (CWBIO, Beijing, China), these mixtures were denatured at 100°C for 20 min. 10μL of protein per lane were separated by 8%, 10%, or 12% sodium dodecyl sulfate-polyacrylamide (SDS-PAGE) gel and transferred to 0.45mm PVDF membrane (Millipore, Shanghai, China). The membrane was then blocked in 5% skim milk solution for 1h at room temperature and then incubated with specific antibodies overnight at 4℃. The primary antibodies included anti-Bmal1 (ab230822, Abcam, 1:2000), anti-VEGF (ab46154, Abcam, 1:2000), anti-VEGFR2 (26415-1-AP, Proteintech, 1:800), anti-MMP2 (10373-2-AP, Proteintech, 1:1000), anti-MMP9 (10375-2-AP, Proteintech, 1:1000), Angiogenin (18302-1-AP, Proteintech, 1:800), anti-Notch1 (10062-2-AP, Proteintech, 1:1500), anti-Hey1 (19929-1-AP, Proteintech, 1:2000), anti-Hes1 (A0925, Abclonal, 1:1500), anti-Jag1 (DF8269, Affinity, 1:1000), anti-DLL4 (A12943, Abclonal, 1:1500), and anti-β-actin (66009-1-Ig, Proteintech, 1:8000). The next day, the membrane was incubated with anti-rabbit horseradish peroxidase- (HRP-) conjugated secondary antibodies (E-AB-1003, Elabscience, China) for another 1.5 hours at room temperature. The Efficient Chemiluminescence Kit (GEN-VIEW, Beijing, China) was used for signal detection and the results were recorded by Bio-Rad ChemiDoc MP Gel Imaging System. The band density of specific proteins was quantified after normalization with the density of β-actin.

2.21 Statistical analysis

Data are presented as the mean ± SD from at least three independent experiments. Statistical comparisons were conducted with unpaired Student's t-test/one-way ANOVA with posthoc Tukey test/two-way ANOVA with posthoc Sidak test as appropriate, and $p < 0.05$ was considered statistically significant.

3 Result

3.1 Environmental Circadian Disruption Increases Stroke Severity and impaired angiogenesis-related facts in MCAO rats

A precise schedule was used in this study that can lead to temporary misalignment of central and peripheral clock genes during resynchronization and disruption within the central pacemaker itself [21, 31, 34] (Fig. 1A). As shown in Fig. 1B, the dorsal hair of rats with normal circadian rhythm is white, thick, clean, and shiny, while the ECD dorsal hair was greasy, gray-yellow, brittle, and partially shed. Representative brain images of 2,3,5-triphenyl tetrazole chloride (TTC)-stained areas showing infarct volumes in three groups 24h after cerebral ischemia-reperfusion injury (Fig. 1C). Infarct volume and 10-day neurological score were quantified separately, and as expected, infarct volume and neurological score were significantly increased in the ECD group (Fig. 1D, E).

As mentioned above, angiogenesis occupies a large proportion in the collateral circulation and rehabilitation process after cerebral infarction. To further understand the damage mechanism of environmental circadian rhythm disturbance on cerebral infarction, we focused on the effect of ECD on

angiogenesis after cerebral infarction. First, we found that the core biological clock gene Bmal1 showed a fluctuation that first decreased and then increased in the MCAO model. After 24 hours of reperfusion, the expression of Bmal1 protein significantly decreased. On the tenth day, the expression of Bmal1 increased significantly compared with 24 hours (Fig. 2A). HE staining showed the hippocampus, neurons and glial cells were arranged in an orderly manner and had a normal structure. MCAO hippocampal neurons are disordered, the cell membrane is damaged, cell morphology is swollen, a large number of neurons are lost and dead, and some nuclei are dissolved, condensed and pyknotic. Compared with the model group, neuronal cell necrosis, nuclear condensed and pyknotic cell membrane, and structure destruction were all aggravated in the MCAO-ECD group (Fig. 2B). As shown in Fig. 2C, the protein levels of MMP-9 and VEGF, which are closely related to angiogenesis, were significantly upregulated in the MCAO group compared with the Sham group (P<0.05), while the MCAO-ECD group was significantly lower than the MCAO group. (P<0.001).

To further determine the relationship between ECD and angiogenesis, we imaged and quantified CD34. Compared with the sham group, the microvessel density ($CD34^+$/Field) in the cortex and hippocampus was increased in the MCAO group, while that in the ECD intervention group was significantly lower than that in the model group (P<0.05) (Fig. 2D). It is well known that inflammatory cells and cytokines can affect the proliferation and migration of endothelial cells [35, 36], so we next detect the level of serum inflammatory cytokines, including IL-1β, IL-18, and TNF-α. As shown in Fig. 2E, the levels of serum IL-1β (P<0.001), IL-18 (P<0.05), and TNF-α (P<0.01) in the MCAO group were higher than those in the Sham group, and the serum IL-1β (P<0.05) and TNF-α (P<0.01) in MCAO-ECD group were significantly higher than those in the MCAO group (Fig. 2E). More than this, the secretion of melatonin, which plays a critical role in the circadian rhythm in which the central and peripheral clocks operate synchronously [37], controls angiogenesis by regulating the expression of VEGF [38]. Significant reductions in serum VEGF (P<0.001) and melatonin (P<0.05) were also detected in our research (Fig. 2E).

3.2 Core clock gene Bmal1 expression is upregulated in OGD-evoked injury bEnd.3 cells

To investigate the changes of gene expression related to circadian rhythm and angiogenesis in endothelial cells after ischemic injury, we first established a bEnd.3 cell OGD/R model to mimic ischemia and reperfusion in vitro. We first intervened bEnd.3 cells with dexamethasone for 2 hours to induce cell cycle synchronization, followed by 6 hours of OGD treatment, and detected the changes of Notch1 intracellular domain (NICD), Bmal1 protein at different time points. As shown in Figs. 3A, B, C, the protein level of Bmal1 and NICD expression was significantly upregulated at 12h and 20h, respectively, in the OGD-evoked injury bEnd.3 cells(P<0.01). More than this, we further explored the changes of angiogenesis related gene expression patterns, including Notch1 and VEGF mRNA were detected by qPCR. The results are shown in Fig. 3, the Notch1 mRNA level in the OGD group began to increase 4 hours after the OGD treatment, and the rhythm oscillation was strengthened. As for VEGF, except for the 12th and 16th hours after OGD treatment, the level of VEGF mRNA increased to varying degrees at each time point, and the amplitude of circadian oscillations was significantly enhanced. (Fig. 3D).

3.3 Genome-wide characterization of core circadian clock Bmal1 transcriptional binding sites in bEnd.3 cells

Bmal1 has been proved as a proangiogenic TF in endothelial cells. However, the genomic binding pattern of Bmal1 in endothelial cells remains unclear. To decipher the regulatory roles of Bmal1 in endothelial cells, in our study, we performed ChIP-seq to determine genome-wide target sites of Bmal1 in bEnd.3 cells. All three biological replicates showed high correlation scores > 0.8 (Fig. 4A). The peaks over chromosomes showed different peak values, among them, there were the most enriched peaks on chromosome 1, and there were the most high values of the peaks on chromosomes 5, 11, 14, and 15 (Fig. 4B). A total of 13006 Ch-IP regions corresponding to 9100 unique Ref-Seq genes were identified (Fig. 4C). Bmal1 binding sites at promoter transcription start sites (TSS) accounted for 7.77% of the total reading (Fig. 4D). Gene ontology (GO) analysis of peak-related genes revealed that Bmal1 target genes were involved in various biological processes such as metabolism, protein modification, and translation initiation (Fig. 4E). Kyoto Encyclopedia of Genes and Genomes (KEGG) analysis revealed that Bmal1 peak-related genes were significantly enriched in cell metabolism, including protein digestion and absorption, phospholipase and phosphatidylinositol pathways, and enriched in gap junction, axon guidance, and focal adhesion pathway, which promote intercellular communication and migration (Fig. 4F). We next performed de novo motif discovery to investigate motifs shared between sequencing peaks and selected the five motifs with the most significant differences in presentation (Fig. 4G). Transcriptional factors can combine with these motifs, and the corresponding relationship between TFs and genes is drawn to map the interaction network (Fig. 4H).

VEGF and Notch signaling pathway plays a critical role in angiogenesis, our in vivo research demonstrated that circadian rhythm disruption impaired the angiogenic ability, and the previous has confirmed that overexpression of the core circadian clock Bmal1 significantly promotes angiogenesis of various endothelial cells. Similarly, we found that Bmal1 binds the enhancer region of Notch1 (position: chromosome2, 26463954–26464324), and downstream gene Hes1(position: chromosome16, 30066868–30067165; 30065082–30065373;30064015–30064496), and binds the promoter region of VEGF (position: chromosome17, 46030452–46030695). Dual-luciferase reporter assay also confirmed that Bmal1 bound directly to the enhancer region of Notch1 in bEnd.3 cells. The construction of the vector is shown in Fig. 8B. 293T cells were transfected with a luciferase expression vector containing Notch1 promoter (– 1478/-1487 -ggacacgcgc-) 5-flanking fragment. Luciferase reporter assay verified that BMAL1 overexpression increased the luciferase activity of Notch1-WT but had no obvious inhibitory effect on that of Notch1-MUT (Fig. 4I).

3.4 Stable overexpression and silencing of Bmal1 bEnd.3 cells were established

To determine the exact effect of the core circadian clock Bmal1 on the angiogenesis process, three kinds of bEnd.3cells were established, including NC (control scramble transfected cells), OE (Bmal1 gene overexpressing cells), and KD (BMAL gene knockdown cells). Bmal1-OE, Bmal1-KD, and negative control lentivirus were all transfected into bEnd.3 cells. After 72H transfection, green fluorescent protein (GFP)

was observed under the fluorescence microscope, and it was confirmed that the transfection efficiency was approximately 97% before proceeding to the next step of detection (Fig. 5A). Then, the relative expression of Bmal1 mRNA and protein in transfected cells was verified by RT-qPCR and western blotting. The results of qPCR showed that among the three designed siRNAs, the knockdown efficiency of Si2 reached more than 50%, and the expression level of overexpressed Bmal1 mRNA was more than 8 folds than that of the NC group. (Fig. 5B). In Figs. 5C, D, SiRNA2 significantly knocked down the protein expression of Bmal1, while the expression of Bmal1 in the OE group was significantly increased. Therefore, we chose siRNA2-knockdown bEnd.3 cells as the object of the follow-up experiment. It was found by immunofluorescence that the expression of Bmal1 in the nucleus of the OE group was significantly increased, while that of the siRNA2 group was significantly decreased. (Fig. 5E).

3.5 Bmal1 is required for endothelial angiogenesis in vitro

We further tested the hypothesis that Bmal1, the core clock gene of circadian rhythm, regulates the endothelial cell angiogenesis process according to the phenotype of circadian rhythm and angiogenesis in Figs. 1–4. Since angiogenesis is a multistage process during which activated ECs sprout, migrate, proliferate, align, form a tube, and anastomose, therefore, tube formation assay, migration assay, and wound healing assay were performed to reproduce these steps. The tube formation assay was conducted to test the angiogenic ability of bEnd.3 cells. In our body, endothelial cells are surrounded by the basement membrane, a thin and highly specialized extracellular matrix (ECM). When endothelial cells are inoculated on basement membrane-like surfaces such as Matrigel, they form capillary-like structures in vitro that reproduce angiogenesis. The transwell and cell scratch wound assays were conducted to test the migration ability of ECs. Due to the certain permeability of the polycarbonate membrane, the complete medium in the lower layer can affect the cells in the upper chamber, thereby reflecting the ability of cell chemotaxis and cell migration. Similarly, cell migration can also be reflected in wound healing assays. A blank region is created on the fused monolayer of cells, and the cells at the edge migrate to the center after receiving a migration signal or sensing a gradient of proangiogenic regulatory factors, such as VEGF. The results revealed that Bmal1 depletion impaired the endothelial angiogenic ability, including tube formation, transwell, and wound healing as shown in Figs. 6A, B, C.

To explore potential downstream effectors that might influence the Bmal1 loss-of-function phenotype, we investigated two known signaling pathways of ECs, namely, VEGF-A and Notch-1-DLL4 signaling pathways, by RT-qPCR. Overexpression of Bmal1 increased expression of angiogenesis-related factors, including VEGF (P<0.001), MMP2(P<0.001), MMP9(P<0.05), and ANG(P<0.05) (Fig. 6D). After knockdown of Bmal1, the expression of VEGF was significantly decreased (P<0.05). Notch1 signaling pathway plays a key role in angiogenesis and maintenance of vascular homeostasis, so the Notch receptor DLL4, ligand JAG1, and several Notch target genes including Hey1 and Hes1 were detected by RT-qPCR. It is worth mentioning that we found that Notch1(P<0.05), DLL4(P<0.01), Hes1(P<0.01), Hey1(P<0.001) were increased in the Bmal1-OE group compared with the NC group. However, the downstream genes of Notch1 remained unchanged in the Bmal1-KD bEnd.3 cell line (Fig. 6E). Overall, the stable Bmal1-

knockdown cell line significantly reduced the ability of angiogenesis and downregulated angiogenic factors, and the results support the pivotal role of Bmal1 in bEnd.3 cells involved in angiogenesis.

3.6 Overexpression of Bmal1 promotes the proliferation and accelerates the angiogenesis ability of OGD injured bEnd.3 cells by regulating the VEGF/Notch1 signaling pathway

To evaluate the exact effect of Bmal1 on angiogenesis after ischemic stroke. We simulated the pathophysiological mechanism of ischemic stroke and constructed an in vitro OGD model of bEnd.3 cells, a series of in vitro function measurements including CCK8, scratch wound assay, migration assay, and tube formation assay were used in this study.

Cells in all groups were incubated in the 96-well plate, the cell proliferation at 24h, 48h, 72h, and 96h was detected by CCK8 assay (Fig. 7A). The result showed that there was no significant difference among the three groups at 24h, 48h (P>0.05). Bmal1-OE group showed a significant difference in cell proliferation rate at 72h and 96h compared with the NC group(P<0.05). There was no significant difference in cell proliferation between CON and NC groups (P>0.05). Wound healing assay, tube formation assay and transwell assay further confirmed the ability of Bmal1 to promote hypoxia-induced angiogenesis. We found that under normoxic conditions, the overexpression of Bmal1 significantly enhanced the migration ability of cells (P<0.01), but in the tube formation and wound healing assays, no obvious promotion was observed. The results of wound healing assay, tube formation assay, and transwell assay showed that under hypoxic conditions, the pro-angiogenic capacity of bEnd.3 cells enhanced due to the massive secretion of VEGFA, VEGFR2, MMP2, MMP9 and ANG. And this promotion effect is further strengthened in bEnd.3 cells overexpressing Bma11, regardless of the migration ability or the tube-forming ability are enhanced to varying degrees (Fig. 7B, C, D).

To further elucidate the protective mechanism of Bmal1 on bEnd.3 cells at the molecular level, we detected angiogenesis and Notch1 signaling pathway-related proteins in bEnd.3 treated with OGD/R by immunofluorescence and western blot. Immunofluorescence assay showed that overexpression of Bmal1 could further upregulated the protein expression of VEGF and Notch1 in both the cytoplasm and the nucleus of hypoxia-induced neovascularization (Fig. 7E-G). Moreover, we further detected angiogenesis related proteins by western blot, and the results suggested that overexpression of Bmal1 can upregulate the protein levels of VEGF (P<0.05) and MMP2 (P<0.01) under normoxia, and the increased protein expression induced by hypoxia could be further enhanced by Bmal1, including VEGF (P<0.001), VEGFR2(P<0.05), MMP-2 (P<0.001), MMP-9(P<0.05) (Fig. 7H). Similarly, the protein levels of NICD (P<0.05) and DLL4 (P<0.05) were upregulated in Bmal1 overexpressed bEnd3 cells. With the severity of OGD / R injury, the protein levels of Notch-1 intracellular domain (P<0.001), related receptors Dll4 (P<0.01), and downstream proteins Hes1 (P<0.05) and Hey1 (P<0.05) were significantly increased. And overexpressed Bmal1 can further increase the expression of NICD (P<0.01), related receptors Jag1 (P<0.01), Dll4 (P<0.05), and downstream proteins Hes1 (P<0.05) and Hey1 (P<0.01) protein compared with ctrl group under hypoxic condition (Fig. 7I).

3.7 Inhibited Notch1 signaling pathway reverses the effect of overexpressed Bmal1 on angiogenesis viability of OGD injured bEnd.3 cells

To further determine whether the Notch 1 signaling pathway is involved in Bmal1 to promote VEGF expression and regulate angiogenesis, we used DAPT to intervene bEnd.3 cells in subsequent studies, evaluating the role of Notch1 in this process by detecting the phenotype of angiogenesis and key protein. DAPT is a potent γ-secretase inhibitor that inhibits the activation of Notch 1 signaling. Therefore, in phenotypic experiments, we added DAPT at the beginning of 24-hour serum shock-induced cell cycle synchronization to inhibit Notch signaling pathway activation, and the intervention of DAPT continued until the end of the phenotype experiments. Under hypoxic conditions, DAPT can significantly reduce the migration ability (P<0.01) and tube-forming ability (P<0.01) of endothelial cells (Fig. 8A, C). Consistent with the previous results, Baml1 significantly promoted the migration ability of endothelial cells in scratch wound (P<0.05), transwell (P<0.001), and tube formation assay (P<0.05), but this promotion was partially reversed by DAPT (10μM). As shown in Figs. 8A, B, C, DAPT inhibited the pro-angiogenic effects of Bmal1, including migratory and tubulogenesis, and we observed a significant reversal in all three phenotypic experiments (P<0.001). Western blot was further used to detect the protein expression closely related to the angiogenic process. First, we detected the protein level of NICD to verify the inhibitory effect of DAPT. The results showed that DAPT could inhibit the activation process of NICD regardless of whether Bmal1 was overexpressed or not (Fig. 8D). Then the key molecules of angiogenesis were detected by western blot, as shown in Fig. 8D, the expression of VEGF decreased after DAPT intervention, and the related proteins including MMP-2 (P<0.01), MMP-9 (P<0.01), ANG (P<0.01), and VEGFR2 (P<0.01) were down-regulated to varying degrees. The results in this section revealed that the Notch1 signaling pathway plays a very pivotal role in the process of Baml1 regulating angiogenesis, and its potential mechanism may be a bridge between Bmal1 and VEGF.

4 Discussion

A growing body of literature suggests that the molecular, cellular, and physiological pathways of circadian rhythm are strongly associated with clinical outcomes in stroke [20]. Elucidating the complex and multifactorial influences of circadian rhythms may improve opportunities for clinical translation in stroke diagnosis and treatment. Changes of the light cycle can lead to ECD, causing a misalignment of the peripheral clock, negatively affecting the functioning of healthy organs, accelerating the pathological process of various diseases [21, 31, 39, 40]. A prior Cox proportional hazards model showed that shift workers were positively associated with the severity of ischemic stroke risk [41], suggesting that shift work leads to increased stroke risk and is an independent risk factor for ischemic stroke [42]. In animal models, phase-advancing light cycles increased the severity of stroke in MCAO/R rats [43].

Therefore, we mimic the circadian disruption of inverted shift work via 6-h weekly advances in the 12:12 photoperiod, promoting rapid phase changes in the SCN, followed by changes in surrounding organs, and adjusting at different rates [44, 45]. Here, the ECD model was successfully established before the MCAO operation. In subsequent experiments, we assessed how advanced changes in the environmental LD

cycle affect neural function and angiogenesis repair after ischemic injury. In an 8-week longitudinal study, we assessed neurological recovery at various time points after middle cerebral artery ischemic injury in rats, collecting brain and serum samples at 24 hours and 10 days after infarction. The results showed that ECD increased the volume of cerebral infarction, as well as aggravated the degree of postoperative neurological injury, and impaired the ability to recover.

Angiogenesis is one of the key processes in the recovery mechanism of ischemic stroke, involving MMPs-induced basement membrane degradation, VEGF-promoted cell proliferation, migration and other functions [46]. Moreover, early zebrafish studies found that continuous light and the intervention of Bmal1 disrupted the circadian rhythm, thereby impairing developmental angiogenesis in zebrafish. It was further found that Bmal1 regulates the expression of VEGF and targets the VEGF gene promoter through e-box region, which strictly regulates the development of blood vessels [47]. Our rat research further found that ECD aggravated the pathological changes of MCAO, including the degree of cortical and hippocampal edema and neuronal damage in the infarcted hemisphere. More than this, ECD impaired the ability of angiogenesis, the positive number of CD34 in the infarcted hemisphere decreased significantly, and the expression of angiogenesis-related factors such as MMP-2 and VEGF decreased. Collectively, this data suggested that the transient dampening of rhythms during misalignment induced by light cycle changes may underlie neurological and vascular dysfunction in the brain, reducing resilience to pathological damage of hypoxia during shift workers and ECD animal models.

Numerous studies have repeatedly shown that inflammation has a multistage and complex role in the development and pathogenesis of ischemic stroke [48]. Although proinflammatory cytokines such as IL-1β and TNF-α can promote angiogenesis, excessive proinflammatory cytokines can adversely affect the progression of angiogenesis [35, 36]. Therefore, we detected the level of IL-1 β, IL-18, and TNF- α in rat serum by ELISA, to explore the relationship between inflammation and angiogenesis. Interestingly, inflammatory factors were significantly increased in the ECD group compared with the non-ECD group, and it was the excessive secretion of inflammatory factors that aggravated the neurological damage and impaired angiogenesis in MCAO rats. At the same time, as a key molecule regulating circadian rhythm, melatonin can also affect angiogenesis in different scenarios by regulating the expression of VEGF and VEGF receptors [38]. In our study, we found that ECD decreased serum melatonin and VEGF levels, and the potential relationship between the two may be that melatonin downregulation leads to decreased VEGF secretion, which in turn impairs angiogenesis after cerebral infarction.

Based on the above research in vivo, we found that biological rhythm regulates the process of angiogenesis after ischemic stroke and affects pathological process to a certain extent. As the core transcriptional factor, Bmal1 regulates the circadian pattern of downstream gene expression [49]. Besides this, Bmal1 has been shown to promote angiogenesis in ischemia-injured HUVECs (human umbilical vein endothelial cells) [50]. However, there is little evidence about the transcription function and epigenetic regulation of Bmal1. In the following experiment, we provide compelling evidence for the molecular mechanisms of how the circadian clock regulates repair angiogenesis following hypoxic injury. First, significant elevations of the core circadian clock Bmal1 were observed in both MCAO rats and OGD

intervened bEnd.3 cells. Then, ChIP sequencing was used to detect the binding sites of Bmal1 on chromatin in bEnd.3 cells, elucidated the genome-wide characterization of Bmal1, and confirmed the transcriptional regulation of Bmal1 in angiogenesis. However, whether the transcriptional activity of Bmal1 differs in different tissues and cells, and whether it is related to the formation of transcriptional complexes with other proteins and genes, such as Clock-Bmal1 heterodimers, remains to be further investigated. We next showed that Bmal1 was required for the proliferation and angiogenesis ability of bEnd.3 cells in normoxia condition by detecting the wound healing, transwell and tube formation assays. And under the hypoxia condition, Bmal1 performed a promoting effect on angiogenesis, by increasing the expression of VEGF and angiogenesis-related molecules.

The Notch pathway is a highly conserved intercellular signaling pathway, which is critical for the development process of human tissue, organ, and phylogeny [51]. Receptors on the cell membrane could be activated and subjected to the sequential proteolytic cleavage once the Notch ligand binds it, then the Notch intracellular domain (NICD) released, which entered the nucleus to activate the transcriptional process of the target gene including Hey-1 and Hes-1, by complexing with the DNA-binding protein RBP-J and mediating the recruitment of histone acetylases and the transcriptional coactivator mastermind-like (MAML) [52]. Notch signaling limits vascular germination by limiting the formation of endothelial tip cells and maintaining arterial properties that depend on their relationship with VEGF [53]. In particular, the Notch signal is activated in endothelial cells in response to ischemic stimulation and further participates in the formation of collateral networks of ischemic stroke [29, 54]. In our research, we found that the NICD, Hes1, Hey1, and related receptors, such as Jag1 and DLL4 protein levels were upregulated in the OGD/R group, and further increased in the group of overexpression of Bmal1. The results of ChIP-seq and dual-luciferase also confirmed that Bmal1 targets the regulation of Notch1 and Hes1 transcription in bEnd.3 cells. In previous studies, to determine the role of Notch1 signaling pathway in cerebral infarction injury, gamma-secretase inhibitor was often used to block Notch1 pathway. Interestingly, DAPT showed favorable pro-angiogenic effects in vivo, promoting poststroke brain remodeling by elevating CBF level [55], whereas DAPT abolished the pro-angiogenic effects of HUCMSCs (human umbilical cord mesenchymal stem cells) in vitro [56]. To verify whether Notch1 activation is involved in pro-angiogenic effects of Bmal1 in bEnd.3 cells, DAPT was added to the co-culture medium prior to co-cultivation. The results showed that DAPT significantly abolished Notch1 activation in cells. More importantly, the addition of DAPT significantly reversed the pro-angiogenic effect of Bmal1, as evidenced by inhibition of cell migration, tube formation, and less VEGF-A production.

In general, this is the first study to clarify the correlation between circadian rhythm and the occurrence and development of ischemic stroke, as well as the function and mechanism of Bmal1 in angiogenesis after ischemic stroke. Currently, several strategies have been proposed to correct clock disruption and desynchronization, to restrain the negative consequences if circadian rhythm impacts are unavoidable. These applications mainly include two aspects: environmental modifications and targeting the clock genes. Environmental modifications also contain high intensity of light, activity and therapy during the day and night. Previous experiments proved that the ambient light influences the occurrence and development of diseases. Mice exposed to low dose light (5 lux) at rest phase displayed a reduction of

hippocampal VEGF and BDNF levels, and accompanied by depressive-like symptoms [57]. Thus, environmental light modifications may be a potential therapy for poststroke. More than this, circadian clocks regulate the molecular expression and function state of angiogenesis to various extents, therefore, another therapeutic strategy may be the change of the phase of the circadian clock, by manipulating the rhythmic phase of circadian clocks closer to the physiological state. As we described in this study, increasing the expression of Bmal1 after stroke can promote angiogenesis and the recovery of stroke function. Thus, Bmal1 may also have therapeutic significance in promoting the regeneration of ischemic vascular diseases.

Declarations

Conflict of Interest

The authors declare that the research was conducted in the absence of any commercial or financial relationships that could be construed as a potential conflict of interest.

Author Contributions

DS-Z, LJ-L, and C-G designed and conceived the study. YX-Z, Y-Z, FK-Z, and Q-Y performed the rat and cell experiment. X-Z and L-S performed the analysis of data. YX-Z wrote the manuscript. DS-Z, LJ-L and Z-L critically revised the manuscript. DS-Z, LJ-L and L-S contributed to writing, the review and editing, supervision, and funding acquisition. All remaining authors participated in the analysis of the data and approved the submitted version.

Funding

This research was supported by the National Science Foundation for Young Scholars of China (No. 82004346, 82104766), Natural Science Foundation of Hunan Province (No. 2021JJ30521, 2021JJ40424), Open fund for the first-class discipline of integrated traditional Chinese and Western medicine of Hunan University of Chinese Medicine (No. 2020ZXYJH38 2020ZXYJH39), University-level fund project of Hunan University of Chinese Medicine (No. 2021XJJJ039)

Availability of data and materials

The datasets presented in this study and the original data are available from the corresponding author upon reasonable request.

Acknowledgments

We would like to thank researcher Li-ping for excellent technical support.

References

1. Zhou M, Wang H, Zhu J, et al. Cause-specific mortality for 240 causes in China during 1990–2013: a systematic subnational analysis for the Global Burden of Disease Study 2013. Lancet 2016; 387(10015): 251–272.
2. Global, regional, and national age-sex specific mortality for 264 causes of death, 1980–2016: a systematic analysis for the Global Burden of Disease Study 2016. Lancet 2017; 390(10100): 1151–1210.
3. Wu S, Wu B, Liu M, et al. Stroke in China: advances and challenges in epidemiology, prevention, and management. Lancet Neurol 2019; 18(4): 394–405.
4. Krishnamurthi RV, Feigin VL, Forouzanfar MH, et al. Global and regional burden of first-ever ischaemic and haemorrhagic stroke during 1990–2010: findings from the Global Burden of Disease Study 2010. Lancet Glob Health 2013; 1(5): e259-281.
5. Wang W, Jiang B, Sun H, et al. Prevalence, Incidence, and Mortality of Stroke in China: Results from a Nationwide Population-Based Survey of 480 687 Adults. Circulation 2017; 135(8): 759–771.
6. Hirano T. Evaluation of Cerebral Perfusion in Patients Undergoing Intravenous Recombinant Tissue Plasminogen Activator Thrombolysis. Neurol Med Chir (Tokyo) 2015; 55(10): 789–795.
7. Ruan L, Wang B, ZhuGe Q, Jin K. Coupling of neurogenesis and angiogenesis after ischemic stroke. Brain Res 2015; 1623: 166–173.
8. Jiang X, Suenaga J, Pu H, et al. Post-stroke administration of omega-3 polyunsaturated fatty acids promotes neurovascular restoration after ischemic stroke in mice: Efficacy declines with aging. Neurobiol Dis 2019; 126: 62–75.
9. Uzdensky AB, Demyanenko S. Histone acetylation and deacetylation in ischemic stroke. Neural Regen Res 2021; 16(8): 1529–1530.
10. Bikfalvi A. History and conceptual developments in vascular biology and angiogenesis research: a personal view. Angiogenesis 2017; 20(4): 463–478.
11. Jin F, Zheng X, Yang Y, et al. Impairment of hypoxia-induced angiogenesis by LDL involves a HIF-centered signaling network linking inflammatory TNFα and angiogenic VEGF. Aging (Albany NY) 2019; 11(2): 328–349.
12. Shweiki D, Itin A, Soffer D, Keshet E. Vascular endothelial growth factor induced by hypoxia may mediate hypoxia-initiated angiogenesis. Nature 1992; 359(6398): 843–845.
13. Yang Y, Torbey MT. Angiogenesis and Blood-Brain Barrier Permeability in Vascular Remodeling after Stroke. Curr Neuropharmacol 2020; 18(12): 1250–1265.
14. Krupinski J, Kaluza J, Kumar P, et al. Role of angiogenesis in patients with cerebral ischemic stroke. Stroke 1994; 25(9): 1794–1798.

15. Wei L, Erinjeri JP, Rovainen CM, Woolsey TA. Collateral growth and angiogenesis around cortical stroke. Stroke 2001; 32(9): 2179–2184.
16. Chen J, Zhang ZG, Li Y, et al. Intravenous administration of human bone marrow stromal cells induces angiogenesis in the ischemic boundary zone after stroke in rats. Circ Res 2003; 92(6): 692–699.
17. Logan RW, McClung CA. Rhythms of life: circadian disruption and brain disorders across the lifespan. Nat Rev Neurosci 2019; 20(1): 49–65.
18. Kollias GE, Stamatelopoulos KS, Papaioannou TG, et al. Diurnal variation of endothelial function and arterial stiffness in hypertension. J Hum Hypertens 2009; 23(9): 597–604.
19. Crnko S, Du Pré BC, Sluijter J, Van Laake LW. Circadian rhythms and the molecular clock in cardiovascular biology and disease. Nat Rev Cardiol 2019; 16(7): 437–447.
20. Lo EH, Albers GW, Dichgans M, et al. Circadian Biology and Stroke. Stroke 2021; 52(6): 2180–2190.
21. Ramsey AM, Stowie A, Castanon-Cervantes O, Davidson AJ. Environmental Circadian Disruption Increases Stroke Severity and Dysregulates Immune Response. J Biol Rhythms 2020; 35(4): 368–376.
22. Koyanagi S, Kuramoto Y, Nakagawa H, et al. A molecular mechanism regulating circadian expression of vascular endothelial growth factor in tumor cells. Cancer Res 2003; 63(21): 7277–7283.
23. Sato F, Bhawal UK, Kawamoto T, et al. Basic-helix-loop-helix (bHLH) transcription factor DEC2 negatively regulates vascular endothelial growth factor expression. Genes Cells 2008; 13(2): 131–144.
24. Jensen LD, Cao Y. Clock controls angiogenesis. Cell Cycle 2013; 12(3): 405–408.
25. Luo W, Garcia-Gonzalez I, Fernández-Chacón M, et al. Arterialization requires the timely suppression of cell growth. Nature 2021; 589(7842): 437–441.
26. Lawson ND, Vogel AM, Weinstein BM. sonic hedgehog and vascular endothelial growth factor act upstream of the Notch pathway during arterial endothelial differentiation. Dev Cell 2002; 3(1): 127–136.
27. Liu ZJ, Shirakawa T, Li Y, et al. Regulation of Notch1 and Dll4 by vascular endothelial growth factor in arterial endothelial cells: implications for modulating arteriogenesis and angiogenesis. Mol Cell Biol 2003; 23(1): 14–25.
28. Al Haj Zen A, Oikawa A, Bazan-Peregrino M, et al. Inhibition of delta-like-4-mediated signaling impairs reparative angiogenesis after ischemia. Circ Res 2010; 107(2): 283–293.
29. Cristofaro B, Shi Y, Faria M, et al. Dll4-Notch signaling determines the formation of native arterial collateral networks and arterial function in mouse ischemia models. Development 2013; 140(8): 1720–1729.
30. Castanon-Cervantes O, Wu M, Ehlen JC, et al. Dysregulation of inflammatory responses by chronic circadian disruption. J Immunol 2010; 185(10): 5796–5805.

31. Hill AM, Crislip GR, Stowie A, et al. Environmental circadian disruption suppresses rhythms in kidney function and accelerates excretion of renal injury markers in urine of male hypertensive rats. Am J Physiol Renal Physiol 2021; 320(2): F224-F233.
32. Esposito E, Li W, T Mandeville E, et al. Potential circadian effects on translational failure for neuroprotection. Nature 2020; 582(7812): 395–398.
33. Yang D, Oike H, Furuse M, Yasuo S. Effect of regular and irregular stimulation cycles of dexamethasone on circadian clock in NIH3T3 cells. Chronobiol Int 2022; 39(1): 97–105.
34. Sellix MT, Evans JA, Leise TL, et al. Aging differentially affects the re-entrainment response of central and peripheral circadian oscillators. J Neurosci 2012; 32(46): 16193–16202.
35. Fahey E, Doyle SL. IL-1 Family Cytokine Regulation of Vascular Permeability and Angiogenesis. Front Immunol 2019; 10: 1426.
36. Zhang C, Zhu M, Wang W, et al. TNF-α promotes tumor lymph angiogenesis in head and neck squamous cell carcinoma through regulation of ERK3. Transl Cancer Res 2019; 8(6): 2439–2448.
37. Cipolla-Neto J, Amaral F. Melatonin as a Hormone: New Physiological and Clinical Insights. Endocr Rev 2018; 39(6): 990–1028.
38. Ma Q, Reiter RJ, Chen Y. Role of melatonin in controlling angiogenesis under physiological and pathological conditions. Angiogenesis 2020; 23(2): 91–104.
39. West AC, Smith L, Ray DW, et al. Misalignment with the external light environment drives metabolic and cardiac dysfunction. Nat Commun 2017; 8(1): 417.
40. Ding SL, Zhang TW, Zhang QC, et al. Excessive mechanical strain accelerates intervertebral disc degeneration by disrupting intrinsic circadian rhythm. Exp Mol Med 2021; 53(12): 1911–1923.
41. Brown DL, Feskanich D, Sánchez BN, et al. Rotating night shift work and the risk of ischemic stroke. Am J Epidemiol 2009; 169(11): 1370–1377.
42. Vyas MV, Garg AX, Iansavichus AV, et al. Shift work and vascular events: systematic review and meta-analysis. BMJ 2012; 345: e4800.
43. Earnest DJ, Neuendorff N, Coffman J, et al. Sex Differences in the Impact of Shift Work Schedules on Pathological Outcomes in an Animal Model of Ischemic Stroke. Endocrinology 2016; 157(7): 2836–2843.
44. Yamazaki S, Numano R, Abe M, et al. Resetting central and peripheral circadian oscillators in transgenic rats. Science 2000; 288(5466): 682–685.
45. Davidson AJ, Yamazaki S, Arble DM, et al. Resetting of central and peripheral circadian oscillators in aged rats. Neurobiol Aging 2008; 29(3): 471–477.
46. Tian J, Popal MS, Huang R, et al. Caveolin as a Novel Potential Therapeutic Target in Cardiac and Vascular Diseases: A Mini Review. Aging Dis 2020; 11(2): 378–389.
47. Jensen LD, Cao Z, Nakamura M, et al. Opposing effects of circadian clock genes bmal1 and period2 in regulation of VEGF-dependent angiogenesis in developing zebrafish. Cell Rep 2012; 2(2): 231–241.

48. Zhu H, Zhang Y, Zhong Y, et al. Inflammation-Mediated Angiogenesis in Ischemic Stroke. Front Cell Neurosci 2021; 15: 652647.
49. Míková H, Kuchtiak V, Svobodová I, et al. Circadian Regulation of GluA2 mRNA Processing in the Rat Suprachiasmatic Nucleus and Other Brain Structures. Mol Neurobiol 2021; 58(1): 439–449.
50. Xu L, Liu Y, Cheng Q, et al. Bmal1 Downregulation Worsens Critical Limb Ischemia by Promoting Inflammation and Impairing Angiogenesis. Front Cardiovasc Med 2021; 8: 712903.
51. Liu J, Li Q, Zhang KS, et al. Downregulation of the Long Non-Coding RNA Meg3 Promotes Angiogenesis After Ischemic Brain Injury by Activating Notch Signaling. Mol Neurobiol 2017; 54(10): 8179–8190.
52. Guruharsha KG, Kankel MW, Artavanis-Tsakonas S. The Notch signalling system: recent insights into the complexity of a conserved pathway. Nat Rev Genet 2012; 13(9): 654–666.
53. Noguera-Troise I, Daly C, Papadopoulos NJ, et al. Blockade of Dll4 inhibits tumour growth by promoting non-productive angiogenesis. Nature 2006; 444(7122): 1032–1037.
54. Takeshita K, Satoh M, Ii M, et al. Critical role of endothelial Notch1 signaling in postnatal angiogenesis. Circ Res 2007; 100(1): 70–78.
55. Tian JQ, Zheng JJ, Hao XZ, et al. Dynamic Evaluation of Notch Signaling-Mediated Angiogenesis in Ischemic Rats Using Magnetic Resonance Imaging. Behav Neurol 2018; 2018: 8351053.
56. Zhu J, Liu Q, Jiang Y, et al. Enhanced angiogenesis promoted by human umbilical mesenchymal stem cell transplantation in stroked mouse is Notch1 signaling associated. Neuroscience 2015; 290: 288–299.
57. Walker WH 2nd, Borniger JC, Gaudier-Diaz MM, et al. Acute exposure to low-level light at night is sufficient to induce neurological changes and depressive-like behavior. Mol Psychiatry 2020; 25(5): 1080–1093.

Figures

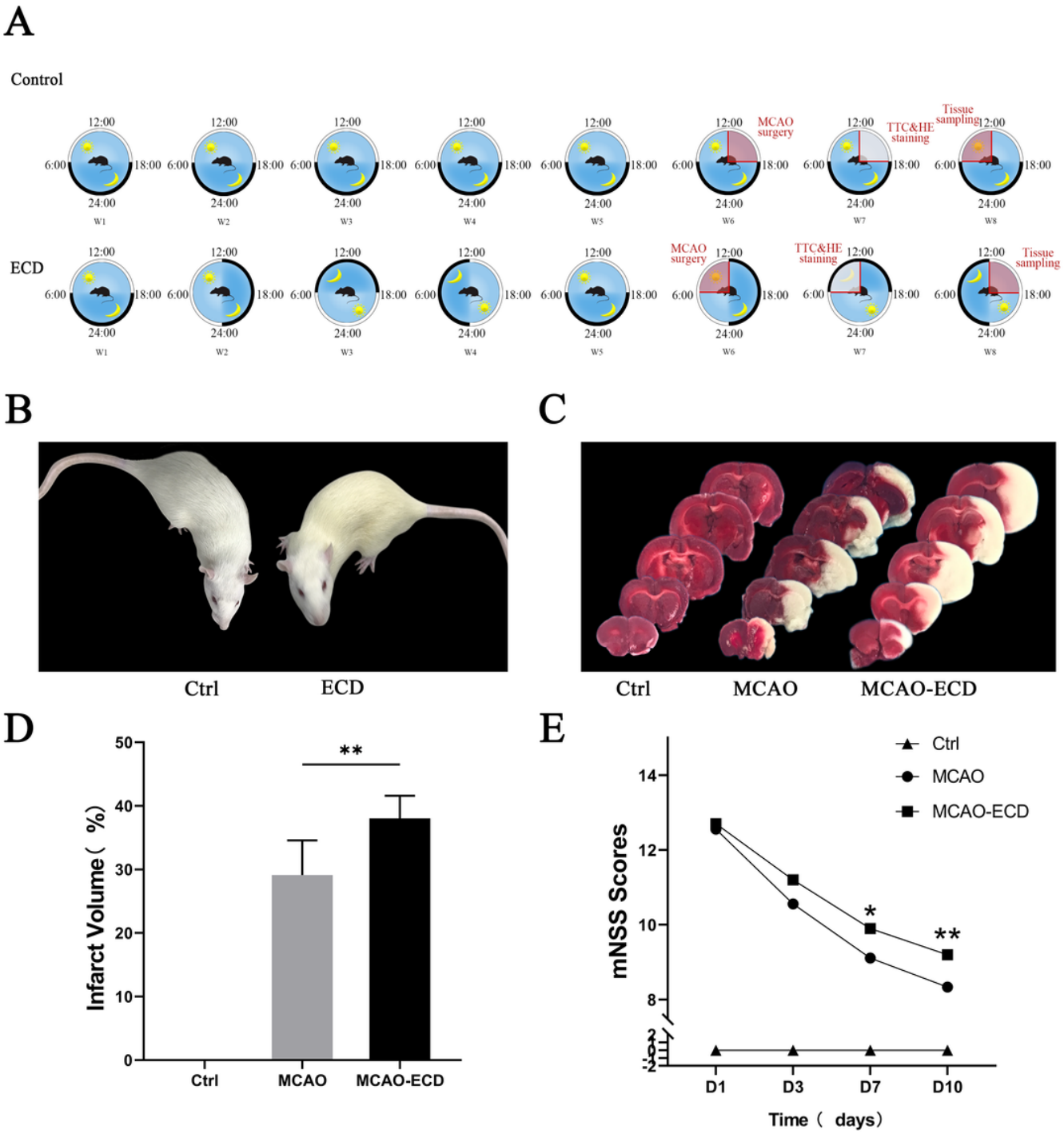

Figure 1

Environmental Circadian Disruption Increases Stroke Severity. A. ECD protocol. Rats were assigned to stay on the standard 12:12 LD schedule, or placed in by shortening the dark period, the 12:12 LD cycle was advanced by 6 hours, once every 7 days for a 44-day (6 weeks). The red range shows the time point of surgery and sampling. **B.** Representative images of the dorsal hair of mice, with non-ECD group on the left and ECD-intervention mice on the right. **C-D.** Representative images and bar graph show the brain lesions in Sham, MCAO, MCAO-ECD, 24h after MCAO surgery (n ≥4). **E.** Bar graphs summarizing the

result of mNSS score in Sham, MCAO, MCAO-ECD (n ≥10). Data are presented as mean. ± SD.*P 0.05, **P 0.01.

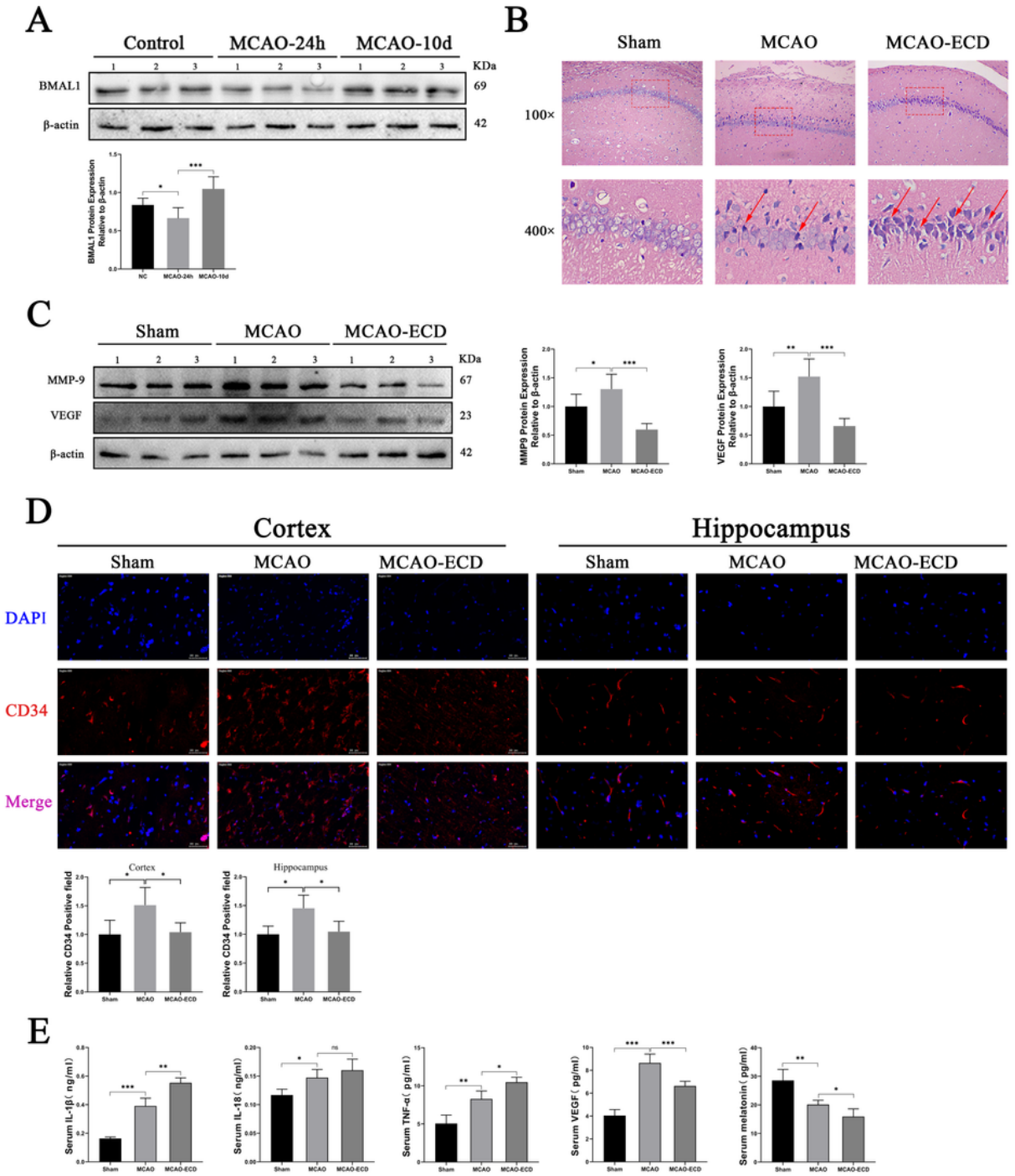

Figure 2

ECD impaired angiogenesis related facts in MCAO rats. A. The changes of Bmal1 protein in brain tissue at different time points were detected by western blot, n=6. **B.** Histopathological changes in hippocampus

tissues of rats in each group were observed by HE staining. The hippocampus tissues of each group rats at 100-fold, 400-fold magnification after HE staining, and necrotic cells indicated by red tips. **C.** The expression of MMP-2, VEGF in brain tissue of each group of rats was determined by western blot (n=6). **D.** Representative immunofluorescence images of CD34 in the hippocampus and cortex 10 days after reperfusion. The sham group was used as the control. Scale bar: 50 μm. **E.** Protein levels of IL-1β, IL-18, TNF-α, VEGF, Melatonin in rat serum were detected by ELISA (n=3). Data are presented as mean ± SD. **P* 0.05, ***P* 0.01, ****P* 0.001.

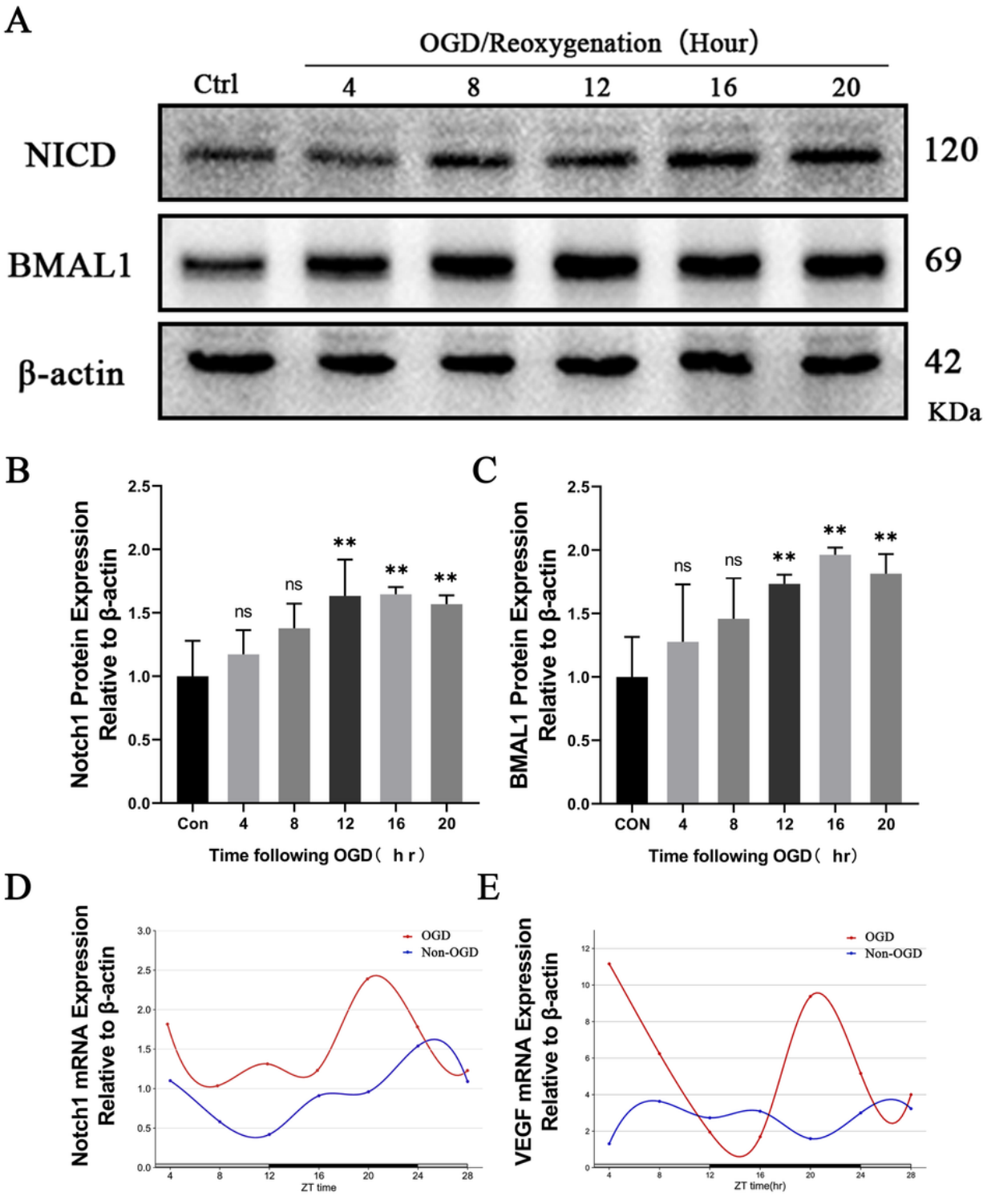

Figure 3

Core clock gene BMAL1 expression is upregulated in OGD-evoked injury bEnd.3 cells. A-C. The expression of NICD and VEGF protein incEnd.3 cells at 4h, 8h, 12h, 16h, 20h after OGD treatment were analyzed by western blot (n=3). **D-E.** The expression of Notch1 and VEGF mRNA in bEnd.3 cells at 4h, 8h, 12h, 16h, 20h after OGD treatment were analyzed by RT-qPCR(n=3). Data are presented as mean ± SD. *P 0.05, **P 0.01, ***P 0.001.

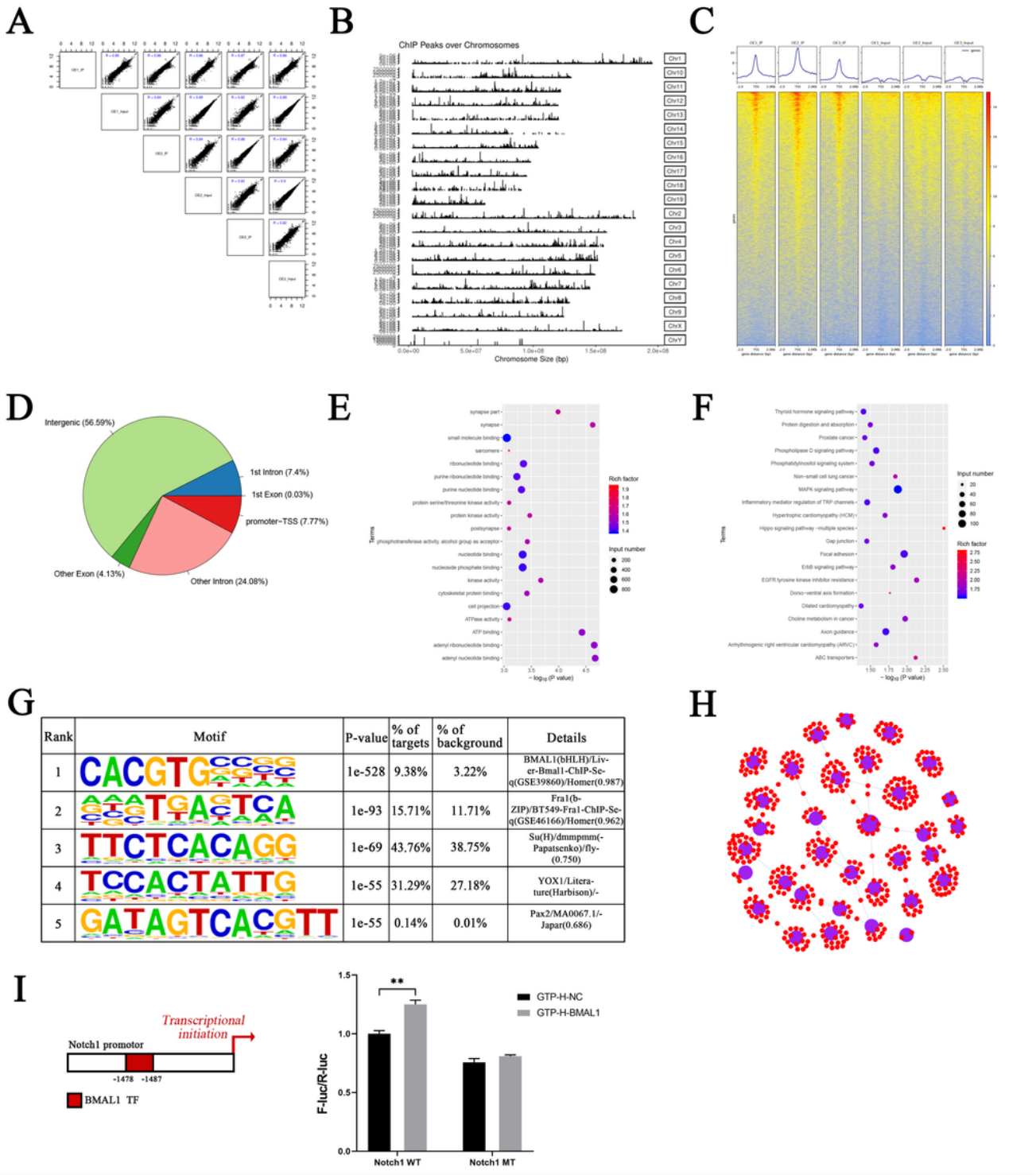

Rank	Motif	P-value	% of targets	% of background	Details
1	CACGTG	1e-528	9.38%	3.22%	BMAL1(bHLH)/Liver-Bmal1-ChIP-Seq(GSE39860)/Homer(0.987)
2	TGACTCA	1e-93	15.71%	11.71%	Fra1(bZIP)/BT549-Fra1-ChIP-Seq(GSE46166)/Homer(0.962)
3	TTCTCACAGG	1e-69	43.76%	38.75%	Su(H)/dmmpmm(-Papatsenko)/fly-(0.750)
4	TCCACTATTG	1e-55	31.29%	27.18%	YOX1/Litera-ture(Harbison)/-
5	GATAGTCACGTT	1e-55	0.14%	0.01%	Pax2/MA0067.1/-Jaspar(0.686)

Figure 4

Genome-wide characterization of core circadian clock Bmal1 transcriptional binding sites in bEnd.3 cells. **A.** All three biological replicates showed high correlation scores >0.8. **B.** Using the primary antibody against Bmal1, peaks were reached on chromosomes by ChIP-seq (The abscissa represents chromosome length, right side represents chromosome number, left ordinate represents the peak value per chromosome). **C.** The distribution of reads on both sides of the transcription start site (TSS). **D.** Pie charts show the ratio of Bmal1 binding sites relative to transcription units, including intergenic, exon 1, intron 1, TTS, promoter, other introns, and other exons. **E.** GO enrichment of Peak related genes (top 20 terms). **F.** KEGG enrichment map of metabolic pathways of Peak-related genes (top 20 terms). **G.** Five common motifs with the most significant differences among peaks. **H.** Interaction network diagram between TFs and genes based on sequencing results, purple represented the transcription factor or transcription factor family, red represented the target gene that TF may act through motifs. **I.** Dual luciferase activity assays were performed using firefly luciferase reporter vectors and renilla luciferase served as an internal control. The experiment was repeated three times. Data are presented as mean ± SD. *, $P < 0.05$; **, $P < 0.01$; ***, $P < 0.001$

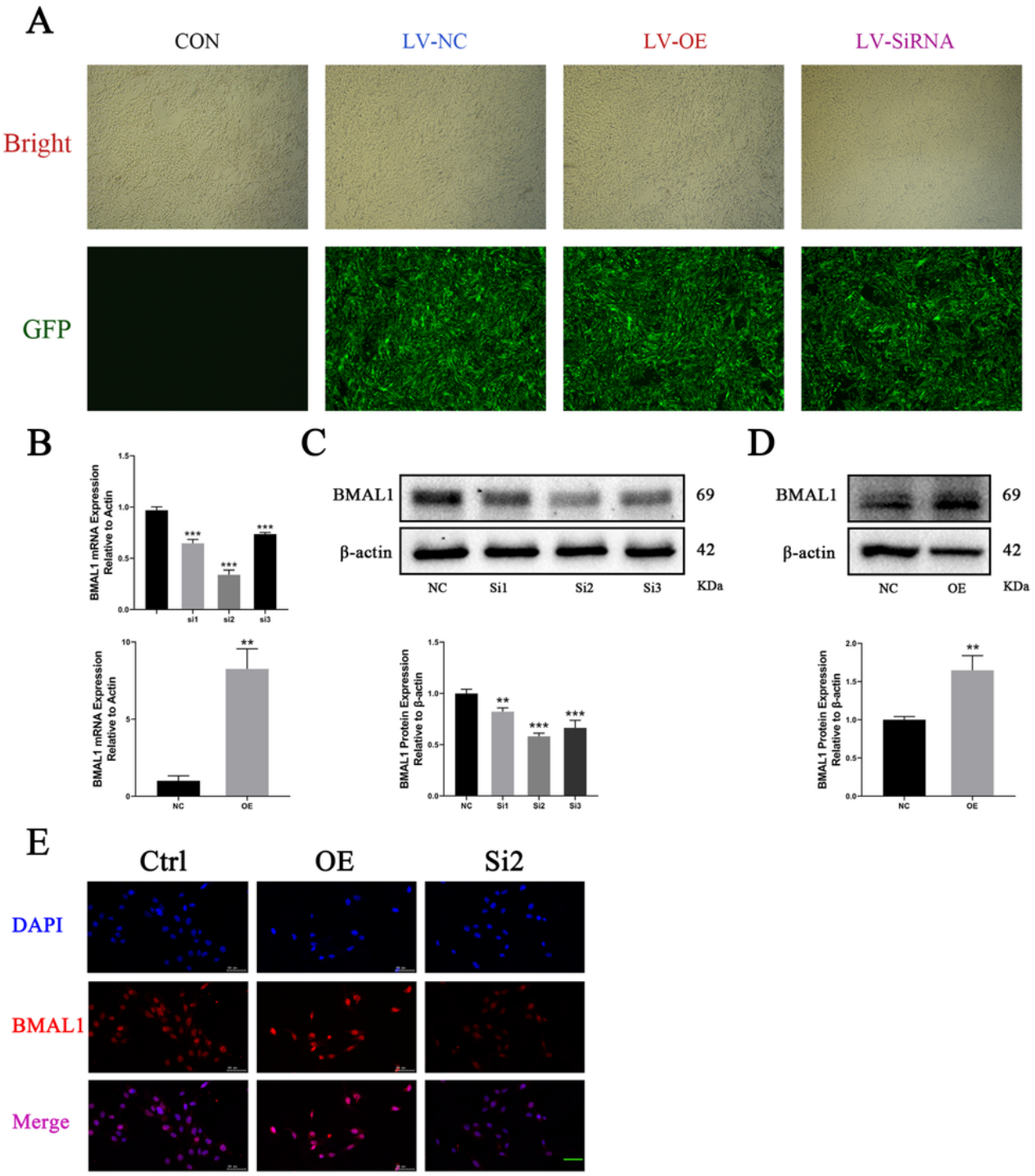

Figure 5

Stable overexpression and silencing of BMAL1 bEnd.3 cells were established. A. The green fluorescent light density indicated that the lentivirus plasmid was highly effectively integrated into the genome of bEnd.3 cells. **B.** RT-qPCR was used, respectively, to detect the mRNA of BMAL1 in SiRNA and OE group. **C.** Western blot results indicating knockdown efficiency verification of three siRNAs (Si1, Si2, and Si3) targeting different sites of BMAL1 in bEnd.3 cells confirmed that Si2 was the most effective siRNA for

knockdown of BMAL1 in bEnd.3 cells. **D.** western blot showed that the BMAL1 protein was overexpressed in OE group. **E.** Representative immunofluorescence images of BMAL1 in bEnd.3 cells. Scale bar: 50 μm. Data are presented as mean ± SD. **P* 0.05, ***P* 0.01, ****P* 0.001.

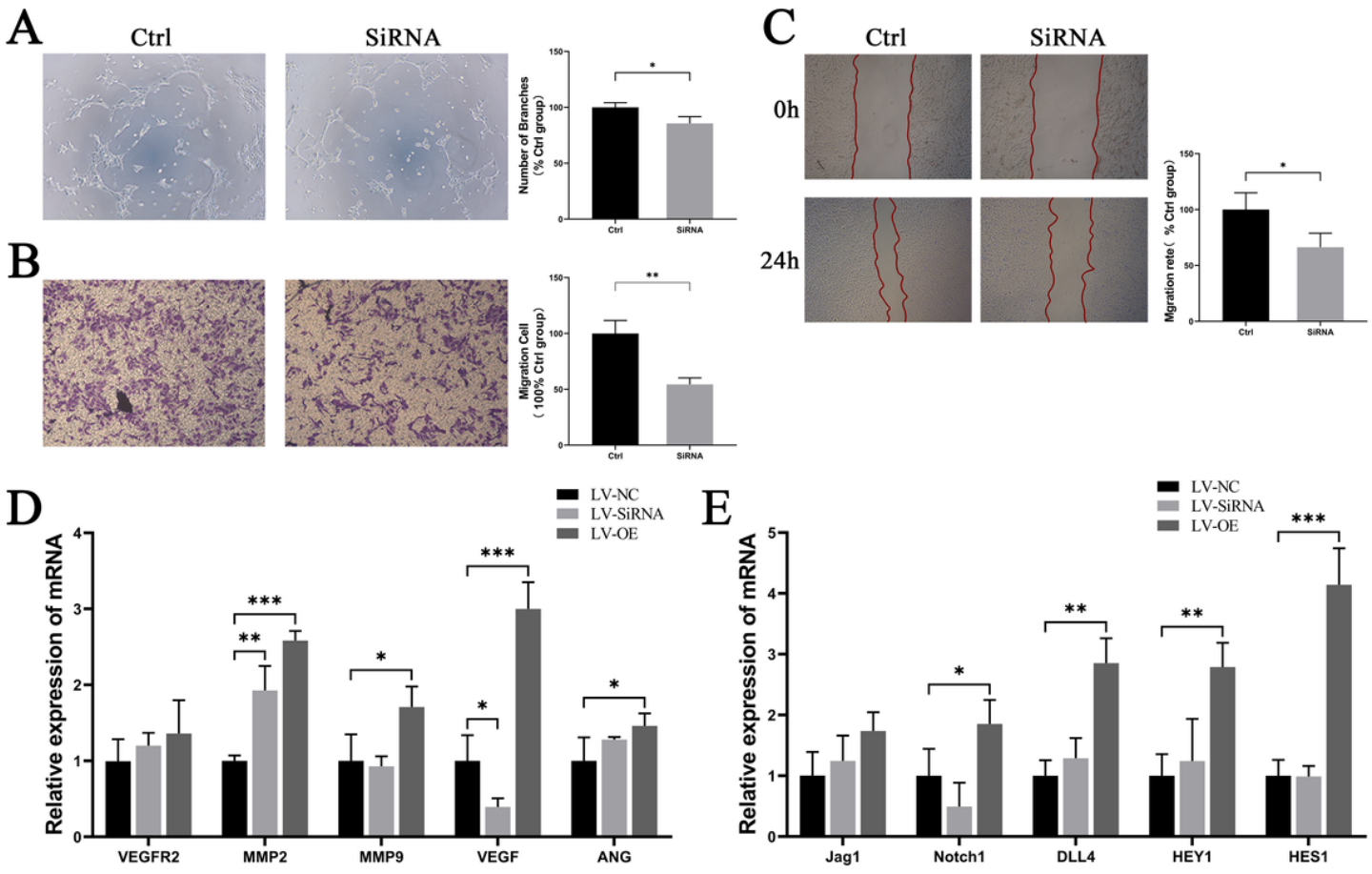

Figure 6

BMAL1 is required for endothelial angiogenesis in vitro. A. Representative microscopic images of tube formation in bEnd.3 cells that transfected with BMAL1 SiRNA. **B.** Phase contrast microscopic images of bEnd.3 cells transfected with BMAL1 SiRNA migrated and attached to the bottom membrane of a transwell. **C.** Phase contrast microscopic images of bEnd.3 transfected with BMAL1 SiRNA at 0 and 24 h after scratching. **D.** The expression of VEGF and angiogenesis related gene mRNA were determined by RT-qPCR. **E.** The expression of Notch pathway and downstream gene mRNA were detected by RT-qPCR. Data are presented as mean ± SD. **P* 0.05, ***P* 0.01, ****P* 0.001.

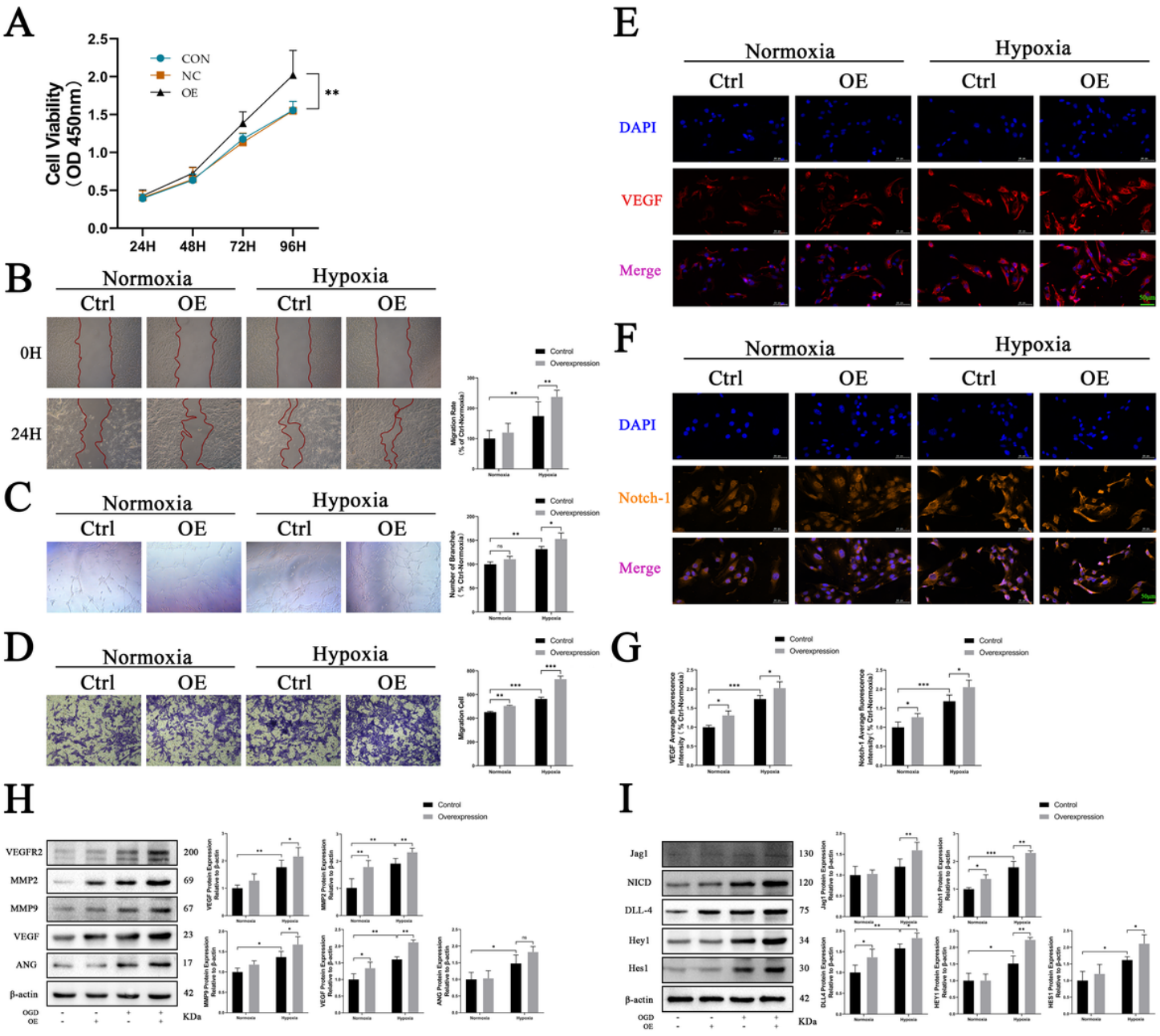

Figure 7

Overexpression of BMAL1 promotes the proliferation and accelerates angiogenesis viability of OGD injured bEnd.3 cells by regulating the VEGF/Notch1 signaling pathway, A. The CCK-8 assay showed that the proliferation of bEn.3 cells were significantly increased when BMAL1 was overexpressed. **B.** Representative microscopic images of bEnd.3 at 0 and 24 h after scratching. **C.** Representative microscopic images of tube formation in bEnd.3 cells. **D.** Phase contrast microscopic images of bEnd.3 cells migrated and attached to the bottom membrane of a transwell. **E-G.** Representative immunofluorescence images of VEGF(E), and Notch1(F) in bEnd.3 cells. Bar chart shows the statistical results from three independent experiments(G). **H.** The expression of VEGF and angiogenesis related gene

proteins were determined by western blot. **I.** The expression of Notch pathway and downstream gene proteins were detected by western blot. Data are presented as mean ± SD. *P 0.05, **P 0.01, ***P 0.001.

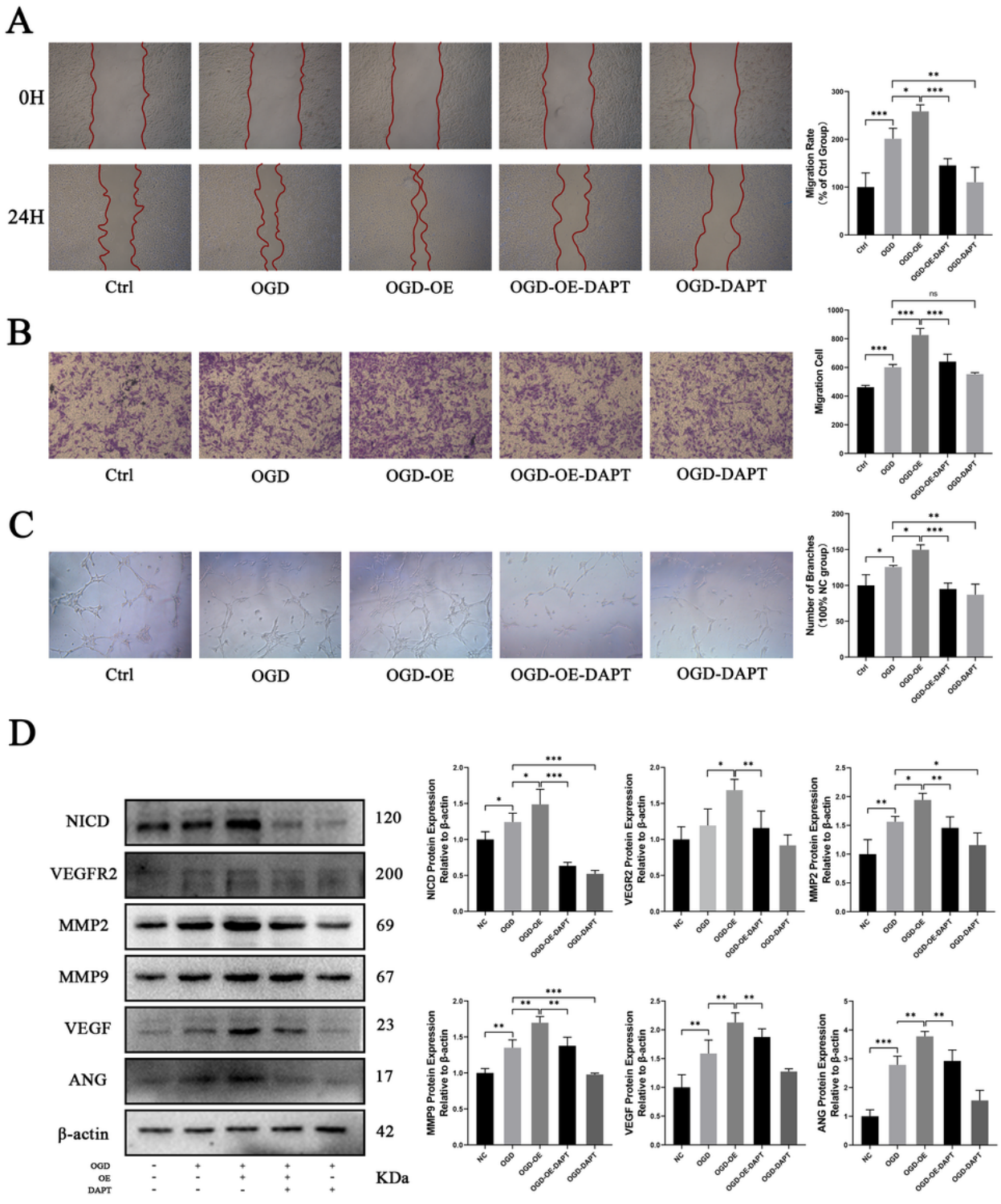

Figure 8

Inhibited Notch1 signaling pathway reverses the effect of overexpressed BMAL1 on angiogenesis viability of OGD injured bEnd.3 cells. A. Representative microscopic images of bEnd.3 cells induced by hypoxia at

0 and 24 h after scratching treated with DAPT. **B.** Phase contrast microscopic images of bEnd.3 cells migrated and attached to the bottom membrane of a transwell induced by hypoxia. **C.** Representative microscopic images of tube formation in bEnd.3 cells induced by hypoxia. **D.** The expression of VEGF, VEGFR2, MMP2, MMP9, and Ang were detected by western blot. Data are presented as mean ± SD. *P 0.05, **P 0.01, ***P 0.001.

Supplementary Files

This is a list of supplementary files associated with this preprint. Click to download.

- supplementalfiles.docx